Tuning competing magnetic interactions with pressure in RMn2O5 multiferroics

W. Peng, V. Balédent, Claire Colin, T. Hansen, M. Greenblatt, P. Foury-Leylekian

Tuning competing magnetic interactions with pressure in $R\mathrm{Mn_2O_5}$ multiferroics

W. Peng,[1,*] V. Balédent,[1] C. V. Colin,[2] T. C. Hansen,[3] M. Greenblatt,[4] and P. Foury-Leylekian[1,†]

[1]*Laboratoire de Physique des Solides, CNRS, Université Paris-Sud, Université Paris-Saclay, 91405 Orsay Cedex, France*

[2]*Institut Néel, CNRS, Université Grenoble Alpes, 38000 Grenoble, France*

[3]*Institut Laue Langevin, 72 Avenue des Martyrs, 38042 Grenoble, France*

[4]*Department of Chemistry and Chemical Biology, Rutgers, The State University of New Jersey, Piscataway, New Jersey 08854, USA*

(Received 16 March 2019; published 6 June 2019)

Magnetoelectric properties displayed in multiferroics are generally associated with complex magnetic orders. This complexity often results in a delicate balance between several geometrically frustrated magnetic exchange interactions. Applying pressure will thus unbalance this equilibrium and strongly affect the multiferroic properties. In this paper, we study the effect of pressure on magnetism in three particular members of the $R\mathrm{Mn_2O_5}$ multiferroics (R = Gd, Sm, and Nd) with interesting magnetic orders. Using powder neutron diffraction, we studied the evolution of their magnetic structures as a function of pressure. Despite their singular properties with respect to the other compositions, we demonstrate that these three members present the same pressure-induced commensurate phase (PCM) with the propagation wave vector [$\mathbf{q}_{\mathrm{PCM}} = (\frac{1}{2}, 0, \frac{1}{2})$]. Furthermore, the stabilization of the PCM phase under pressure can be explained by a similar mechanism. We ultimately conclude that the different origin of the CM and PCM phases of these three compounds are related to the competition of only two superexchange interactions, namely J_1 and J_6.

DOI: 10.1103/PhysRevB.99.245109

I. INTRODUCTION

The presence of different properties in a single material induces the emergence of new phenomena thanks to their coupling. This is the case of magnetoelectric multiferroics which display both magnetic order and ferroelectricity [1]. In this particular case, the very existence of such systems raises fundamental issues as the stabilization of one order usually excludes the other. This explains why these multifunctional materials are so scarce by nature. A magnetoelectric coupling (MEC) induced by the presence of both orders can manifest in both static and dynamical degrees of freedom. A strong MEC, interesting for certain applications, usually appears in improper multiferroics for which the ferroelectricity is induced by the complex magnetic spin structure [2,3].

$R\mathrm{Mn_2O_5}$ compounds (where R is a rare-earth ion, Y or Bi) crystallize in the ferroelectric Pm space group already at room temperature [4]. However, the system is generally described in its average centrosymmetric $Pbam$ space group because the atomic displacements related to the symmetry breaking to Pm are very weak. The structure is formed of $\mathrm{Mn^{4+}O_6}$ octahedra and $\mathrm{Mn^{3+}O_5}$ square-based pyramids. In the (a, b) plane, edge-sharing $\mathrm{Mn^{4+}O_6}$ octahedra and $\mathrm{Mn^{3+}O_5}$ pyramids form pentagons. There are three inequivalent antiferromagnetic (AFM) superexchange interactions between Mn ions in this plane: J_3 and J_4 for the $\mathrm{Mn^{3+} - Mn^{4+}}$ couples, and J_5 between two $\mathrm{Mn^{3+}}$ spins (see Fig. 1). Along the c axis, the structure is made of chains of $\mathrm{Mn^{4+}O_6}$ octahedra separated by layers of $\mathrm{Mn^{3+}O_5}$ pyramids or of R^{3+} ions. There are two different AFM exchange interactions between the $\mathrm{Mn^{4+}}$ spins, J_1 (through the R^{3+} layers) and J_2 (through the $\mathrm{Mn^{3+}}$ layers). The J_2 interaction is strongly frustrated as the two $\mathrm{Mn^{4+}}$ ions are part of four $\mathrm{Mn^{4+} - Mn^{3+} - Mn^{4+}}$ triangles, involving two J_4 interactions and two J_3 interactions. For compounds with large R^{3+} spins, another exchange interaction, J_6, between R^{3+} and $\mathrm{Mn^{3+}}$ moments also has to be considered [5].

The total reversal of the electric polarization by application of an alternated magnetic field in $\mathrm{TbMn_2O_5}$ [6] has drawn much attention for the study of this series of multiferroics. In these compounds, the magnetic structures are characterized by quasicollinear spin arrangements. The ferroelectricity induced by the magnetism thus differs from the standard Dzyaloshinskii-Moriya interaction usually invoked for magnetoelectric multiferroics with noncollinear spins. It has been recently clarified and related to the exchange-striction mechanism [7], which explains the multiferroic properties of all the members of this family.

The magnetic structures in these compounds show a large variety of spin orientations depending on the nature of the R ion. As for the multiferroic properties, one can divide this family into two subgroups with common features, depending on the size of the rare earth. For heavy rare earth ($R >$ Sm) [5,8–15], a succession of magnetic transitions occurs as a function of temperature. The first transition leads to a high-temperature (HT) incommensurate magnetic phase (ICM) with propagation wave vector $(\frac{1}{2}, 0, \frac{1}{4} + \delta)$ and develops below ∼40 K. At lower temperatures, a commensurate magnetic phase ($\mathrm{CM_0}$) with propagation wave vector $(\frac{1}{2}, 0, \frac{1}{4})$ settles down, concomitant with the appearance of the ferroelectricity. Cooling down, the magnetic structure recovers its incommensurate character with a magnetic propagation wave

*Present address: Max Planck Institute for Chemical Physics of Solids, Nöethnitzer Str. 40, 01187 Dresden, Germany.

†Corresponding author: pascale.foury@u-psud.fr

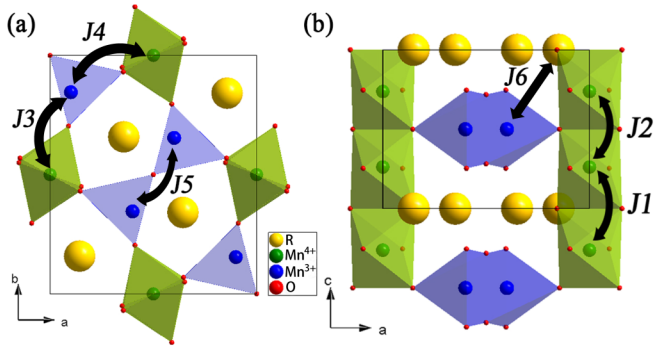

FIG. 1. General crystal structure of $R\mathrm{Mn_2O_5}$. Projections along (a) c and (b) b.

vector $(\frac{1}{2}, 0, \frac{1}{4} + \epsilon)$ close to the one of the HT-ICM phase. In this LT-ICM phase, a strong decrease of the electric polarization is observed. A fourth transition below $T \sim 10$ K appears in some members of the subgroup. It is generally ascribed to the rare earth's spin ordering with the same propagation wave vector as the Mn spins or with a commensurate propagation wave vector $(\frac{1}{2}, 0, 0)$ (CM phase). For light rare earth (from La to Nd) [16–18], ferroelectricity is null or a few orders of magnitude smaller than for the other compounds. Despite this general picture, we can single out some compositions for their specificity. First, $\mathrm{GdMn_2O_5}$ presents an electric polarization one order of magnitude higher than the one of the other members [19], which is attributed to an additional exchange striction mechanism related to the frustration of a $R^{3+} - \mathrm{Mn}^{3+}$ exchange coupling. Second, $\mathrm{SmMn_2O_5}$, which presents the second-highest polarization magnitude [20], has a unique magnetic structure. It presents spins perfectly collinear and aligned along the c axis [7] in contrast with most of the other compositions for which the spins lie in the (a, b) plane [5,21,22]. The third composition, $\mathrm{NdMn_2O_5}$, is ferroelectriclike at ambient pressure, but the polarization is minute [18] and one can speculate as to how to enhance it. For all three members of the series, the influence of the pressure should be of particular interest with regard to the electric polarization.

Recent studies of the magnetic structure as a function of pressure revealed a similar pressure-induced commensurate magnetic (PCM) phase in several members of the family, namely, $\mathrm{YMn_2O_5}$ [23,24], $\mathrm{PrMn_2O_5}$ [25], $\mathrm{DyMn_2O_5}$, and $\mathrm{TbMn_2O_5}$ [26] as well as $\mathrm{BiMn_2O_5}$ [27]. This new phase settles with a propagation vector $(\frac{1}{2}, 0, \frac{1}{2})$. It is interesting to notice that for $\mathrm{HoMn_2O_5}$, this new phase has not been evidenced [28] but the investigation was limited to low pressure (below 1.25 GPa). It progressively takes over the ICM phase and eventually replaces it totally at high pressure. The CM phase present at ambient pressure and low temperature is usually weakened under pressure but is totally replaced only in $\mathrm{PrMn_2O_5}$ [25]. The natural issue arising from the previous results is how the pressure affects the three compositions singled out previously: $\mathrm{GdMn_2O_5}$, $\mathrm{SmMn_2O_5}$, and $\mathrm{NdMn_2O_5}$. In this paper, we present a powder neutron-diffraction (PND) study under pressure of these three compositions.

II. EXPERIMENTAL DETAILS

The measurements presented in this paper were performed on a high-purity and high-quality powder, whose synthesis was carried out following the process described in Ref. [17], starting from a ^{160}Gd-enriched $\mathrm{Gd_2O_3}$ oxide and a ^{154}Sm-enriched $\mathrm{Sm_2O_3}$ oxide, chosen for their low neutron absorption cross section. We used the natural Nd oxide for the synthesis of $\mathrm{Nd_2O_3}$. The PND experiments were conducted on both the D1B and D20 high flux diffractometers at the Institute Laue Langevin (ILL) with a wavelength of $\lambda = 2.42$ Å for D20 and $\lambda = 2.52$ Å for D1b. The metadata of the PND experiments of $^{160}\mathrm{GdMn_2O_5}$ [29], $^{154}\mathrm{SmMn_2O_5}$ [30], and $\mathrm{NdMn_2O_5}$ [31] can be found on the website of ILL. We used a Paris-Edinburgh pressure cell with a sample volume of about 50 mm^3, with ethanol-methanol as the pressure-transmitting medium to obtain hydrostatic compression up to 10 GPa. Lead (Pb) was placed inside the anvil cell enabling pressure estimation using a Pb diffraction pattern combined with its equation of state. The refinement of the nuclear and magnetic structures were carried out using the FULLPROF program [32].

III. RESULTS AND ANALYSIS

A. $\mathrm{GdMn_2O_5}$

The magnetic structure of $\mathrm{GdMn_2O_5}$ at ambient pressure has been recently studied [9]. At ambient pressure below T_1, an HT-ICM phase appears which is replaced below T_{CM} $(p = 0) \approx 35$ K by the majority CM phase with the propagation wave vector $(\frac{1}{2}, 0, 0)$. This low-temperature phase transition is due to the additional magnetic ordering of the R^{3+} spins. It does not change while increasing pressure up to its higher value of 8.4 GPa as shown in Fig. 2(a). Above 6 GPa, the critical temperature $T_{\mathrm{CM}}(\mathrm{p})$ starts to decrease and reaches below ~32 K at 8.4 GPa. In the temperature range between $T_{\mathrm{CM}}(\mathrm{p})$ and $T_1(\mathrm{p})$, an additional magnetic phase appears. As shown in Fig. 3, at 8.4 GPa, when temperature is above 32 K, the PCM starts to appear with the disappearance of the CM phase. The magnetic propagation wave vector of this new pressure-induced phase is indexed with the same propagation vector $\mathbf{q} = (\frac{1}{2}, 0, \frac{1}{2})$ as the PCM phase reported in several other members of the family [23,25,26] and will be labeled PCM phase in the following. The deduced phase diagram from the combination of all our data is summarized in Fig. 4.

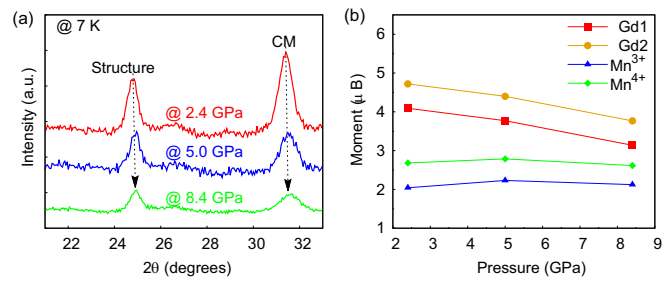

FIG. 2. $\mathrm{GdMn_2O_5}$. Pressure evolution of the CM(p) phase at 7 K: (a) the PND curves at 2.4, 5.0, and 8.4 GPa; and (b) the corresponding amplitude of the moments of Gd^{3+}, Mn^{3+}, and M^{4+}, deduced from the refinements.

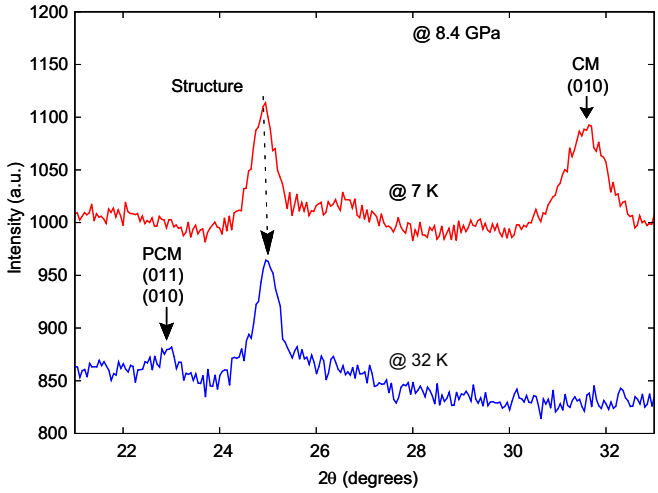

FIG. 3. $GdMn_2O_5$. Temperature evolution of the main reflections of the CM: (010) and PCM: (010) & (011) phases at 8.4 GPa.

It is important to notice that at ambient pressure the reflections of the CM phase are very intense and comparable to the intensity of the nuclear reflections. Their intensity decreases slightly and monotonously with increasing pressure, without any evidence of phase transition. Thus, to refine the CM(p) phase, we used as an initial model the structure of the ambient pressure CM phase described in the P_ab2_1a average magnetic space group [9]. The refinements have been performed at the lowest temperature (7 K), at which the CM(p) phase is the most prominent. By adjusting the amplitude and the direction of the moments using symmetry constraints of the magnetic space group P_ab2_1a, we have obtained good fits of the data for all the pressures studied. The pressure evolution of the

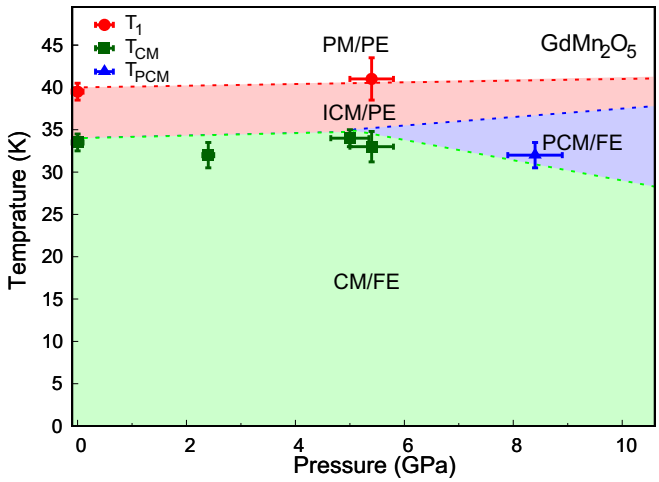

FIG. 4. Pressure–temperature (P-T) diagram of $GdMn_2O_5$ deduced from our neutron-diffraction experiments. The phase boundary at T_{PCM} is arbitrary. It should be between the ICM phase and CM phase and have similar behavior as other compounds ($TbMn_2O_5$, $DyMn_2O_5$ [26], later $SmMn_2O_5$ and $NdMn_2O_5$). The magnetic transition points used for the construction of the phase diagram are determined by the (dis)appearance of the main magnetic reflections [CM: (010) and PCM: (010) & (011)] if there are no other obvious magnetic reflections. This method also applies for the other compounds.

amplitude of the Mn spins and Gd^{3+} moments at 7 K is given in Fig. 2(b). We can see that at low temperatures, the moments of all the ions are not strongly affected by the pressure.

For the refinement of the PCM phase, we considered three models issued from the following symmetry analysis. Within the real HT space group Pm and the magnetic propagation wave vector $\mathbf{q} = (\frac{1}{2}, 0, \frac{1}{2})$, one has two possible irreducible representations, D_1, D_2. It is interesting to notice that a symmetry analysis performed in the higher symmetry space group $Pb2_1m$, the highest compatible with ferroelectricity, yields two irreducible representations with similar constraints as for D_1, D_2. As can be seen in the following, the magnetic moments of either Mn^{3+} (D_1) or R^{3+} (D_2) are along c. But the magnetic structures for this series of compounds generally show spin constraint in the (a, b) plane (except for $SmMn_2O_5$). In addition, magnetization measurements evidence that the (a, b) plane is the magnetic easy plane at least at ambient pressure. All the spins are thus expected to remain in the (a, b) plane in the PCM phase as well. To probe this case, we introduced another magnetic model (*planar* model) for which all the spins are constrained in the (a, b) plane. This last model allowed that the HT space group encounters a symmetry breaking from the Pm to the $P1$ space group as it is probable at the HT-ICM phase transition.

(1) D_1: The magnetic moments of Mn^{3+} are along the c axis, while the magnetic moments of R^{3+} are in the (a, b) plane. No constraints on Mn^{4+} moments' orientations.

(2) D_2: The magnetic moments of Mn^{3+} are in the (a, b) plane, while the magnetic moments of R^{3+} are along the c axis. No constraints on Mn^{4+} moments' orientations.

(3) *Planar*: The spins are all in the (a, b) plane.

The refinement of the data at 32 K and 8.4 GPa in the PCM phase has been performed with these three models. In the refinements, we used the ambient pressure CM phase as a starting point but released the $2'_1$ restriction. For the D_2 model, the directions of the moments were fixed to the one at ambient pressure and only the three amplitudes of the moments were refined. For the *planar* model, we refined the direction of the Gd^{3+} moments and the amplitudes of all the moments. As there are not enough independent PCM reflections, the refinement of the directions of the various spins within these models was difficult and not fully accurate. The results for the various models are presented in Fig. 5. Obviously, the fit with the D_1 model is not good, especially around 16°. The D_2 and *planar* models result in the same quality of refinement and the same reliability factors. However, the planar model seems to be more likely from a physical point of view. First, as discussed above, the magnetic easy plane of most RMn_2O_5 compounds is the (a, b) plane. Second, the absence of spin-orbit coupling for Gd^{3+} [19] makes it sensitive to the molecular field of the Mn ions and align in the (a, b) plane. This is only possible within the planar model. The best fit of the data has been obtained for the magnetic structure shown in Fig. 6 and the refined parameters listed in Table I. Compared to the CM phase, the ordered moments of the Gd ions in the PCM phase are nearly nil (0.2 μB), whereas the amplitude of the moments of Mn ions are similar to the ones of the CM phase at ambient pressure. The weak amplitude of the ordered moments of Gd^{3+} is surprising. However, it is also observed in the PCM phase of $TbMn_2O_5$ and $DyMn_2O_5$ [23,26].

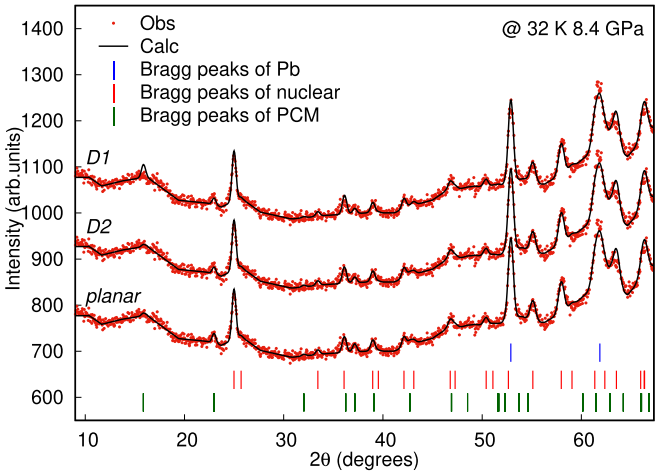

FIG. 5. Diffractogram of $GdMn_2O_5$ at 32K and 8.4 GPa where the PCM phase is present alone.

B. $SmMn_2O_5$

At ambient pressure, below $T_1 \sim 35$ K, an HT-ICM phase is observed in $SmMn_2O_5$. Below $T_2 \sim 28$ K, it is replaced by the CM phase with a propagation wave vector $\mathbf{q} = (\frac{1}{2}, 0, 0)$ which is the main phase. Below ~8 K, another ICM phase (LT-ICM) appears and coexists with the CM phase. In this CM phase at ambient pressure, all the spins are perfectly collinear along c. This quite unusual feature is ascribed to a strong anisotropy of the Sm^{3+} moments with a magnetic easy axis along c [7].

Under pressure, the CM phase persists in the entire pressure range studied, below T_2(p). Furthermore, T_2(p) decreases under pressure. Above a pressure of about 5 GPa, the HT-ICM phase is replaced by a PCM phase with a propagation vector $\mathbf{q}_{PCM} = (\frac{1}{2}, 0, \frac{1}{2})$. This phase is similar to the one observed in YMn_2O_5 [23], $PrMn_2O_5$ [25], $DyMn_2O_5$, $TbMn_2O_5$, [26] and similar to the one we have observed in $GdMn_2O_5$. This PCM phase is stabilized in the entire temperature range below T_1(p)

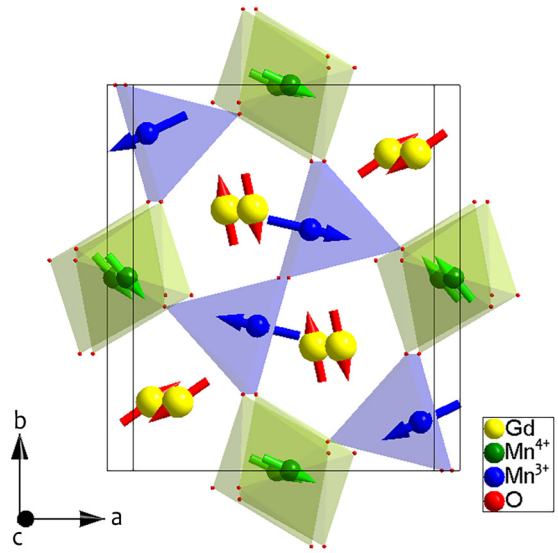

FIG. 6. Magnetic structure of the PCM phase of $GdMn_2O_5$ at 32 K and 8.4 GPa. The amplitude of the moments for Gd^{3+} are multiplied by a factor of 8 for the sake of clarity.

TABLE I. Refined results for the magnetic structure of $GdMn_2O_5$ at 32 K and 8.4 GPa within the *planar* model in the $P1$ space group. $\chi^2 = 1.85$, $R_p = 43.2\%$, $R_{wp} = 27.7\%$, $R_{exp} = 20.1\%$, $R_{bragg} = 4.0\%$, and $R_{mag} = 27.4\%$. ϕ and θ refer to the polar angle and the azimuthal angle, respectively.

Atom	x	y	z	$M(\mu_B)$	$\phi(^\circ)$	$\theta(^\circ)$
Gd^{3+}	0.1354	0.1776	0	0.2(1)	−327.6(2)	90
	0.3645	0.6776	0	0.2(1)	105.2(2)	90
	0.6354	0.3223	0	0.2(1)	105.2(2)	90
	0.8645	0.8223	0	0.2(1)	−327.6(2)	90
Mn^{3+}	0.4187	0.3746	0.5	1.9(2)	−193.6(0)	90
	0.5812	0.6253	0.5	1.9(2)	−13.6(0)	90
	0.1812	0.8746	0.5	1.9(2)	−158.7(7)	90
	0.9187	0.1253	0.5	1.9(2)	−158.7(7)	90
Mn^{4+}	0	0.5	0.2479	1.3(9)	−45.2(7)	90
	0	0.5	0.7520	1.3(9)	−45.2(7)	90
	0	0.5	0.2479	1.3(9)	−21.0(7)	90
	0	0.5	0.7520	1.3(9)	−21.0(7)	90

and coexists with the CM phase below T_2(p). Interestingly T_1(p) strongly increases with pressure and in a quasilinear fashion. This leaves a large portion of the phase diagram to the PCM phase above 5 GPa.

We have investigated in more detail the coexistence of the CM and PCM phases at 15 K as a function of the pressure. To estimate the balance between the two phases, we have calculated the ratio between the integrated intensity of the main magnetic reflections of the CM and PCM phases, respectively (indexation of the main magnetic reflections are shown in Fig. 7). The plot of the pressure evolution of this ratio is represented in Fig. 7. It is worth noting that at 5.5 GPa and above, the ratio between the two magnetic phases at 15 K remains around 50% and that there is no additional significant change in the phase diagram. The corresponding $(P - T)$ phase diagram is summarized in Fig. 8.

We have refined the magnetic phases under pressure starting with the CM(p) phase. At low pressure (below 1.9 GPa), the neutron diffractograms being similar to those at ambient pressure, we expect a CM(p) structure similar to the one at ambient pressure. In particular, we expect the spins remaining perfectly parallel and along the c axis. So, at 15 K and 1.9 GPa, we have only slightly adjusted the amplitude of

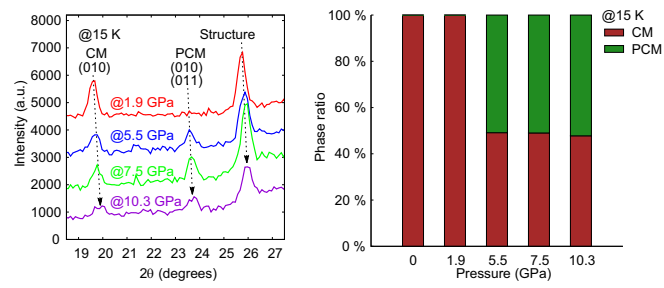

FIG. 7. $SmMn_2O_5$. Diffractograms and phase ratio of the pressure evolution of the CM and PCM phases at 15 K. The phase ratio is calculated via the integrated intensity of the main magnetic reflections [CM: (010); PCM: (010) and (011)] of the two phases.

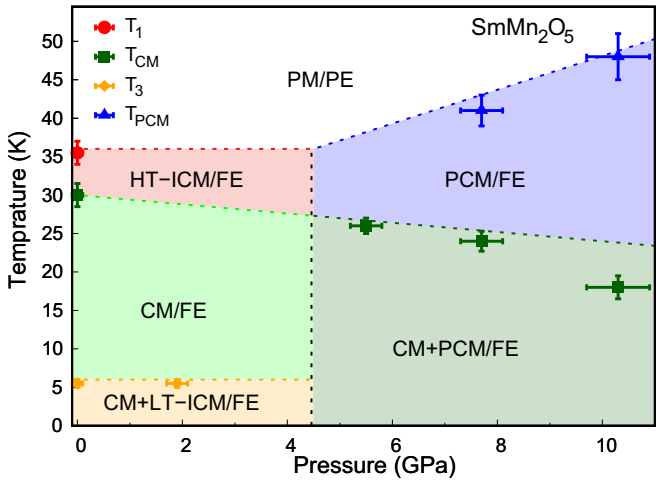

FIG. 8. Pressure-temperature (P-T) diagram of $SmMn_2O_5$ deduced from our neutron-diffraction experiments.

the moments from the ones at ambient pressure and obtained quite good agreement factors ($R_{mag} = 21.6$ %). We obtained 2.7, 1.6, and 0.5 μ_B for the moments of Mn^{3+}, Mn^{4+}, and Sm^{3+}, respectively. This result implies that the magnetic easy axis of the Sm^{3+} moment remains along c under pressure.

The magnetic easy axis of the Sm^{3+} spins remaining along c under pressure, only the D_2 model is relevant for the refinement of the PCM phase. In addition, we ascribed the Mn^{4+} to align in the (a, b) plane as for the Mn^{3+} spins. Indeed, the magnetic anisotropy of the Mn spins favors the (a, b) plane. With these restrictions, a good agreement of the fit with the data has been obtained as presented in Fig. 9. The corresponding magnetic structure of the PCM phase is shown in Fig. 10 and the refined moments are given in Table II. The amplitude of the ordered moments of Sm^{3+} has been found to be 0.7 μ_B. This is close to the value theoretically calculated and experimentally observed at ambient pressure [9]. In addition, it is a small value as usually observed for the ordered moments of the R^{3+} spins in the PCM phase of the other members of the series.

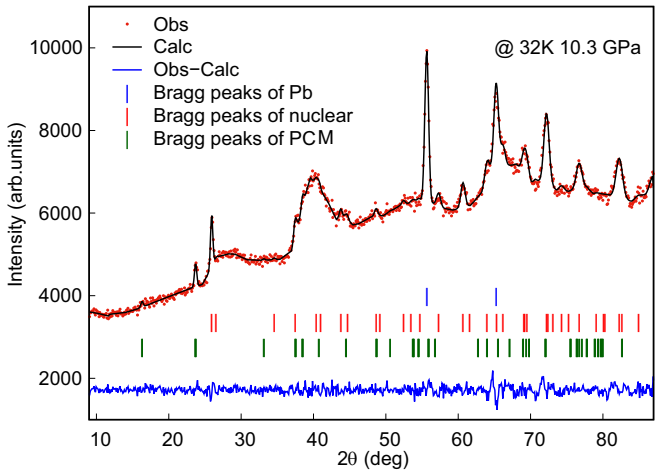

FIG. 9. Diffractogramm of $SmMn_2O_5$ at 32 K and 8.4 GPa, where the PCM phase is the only magnetic phase.

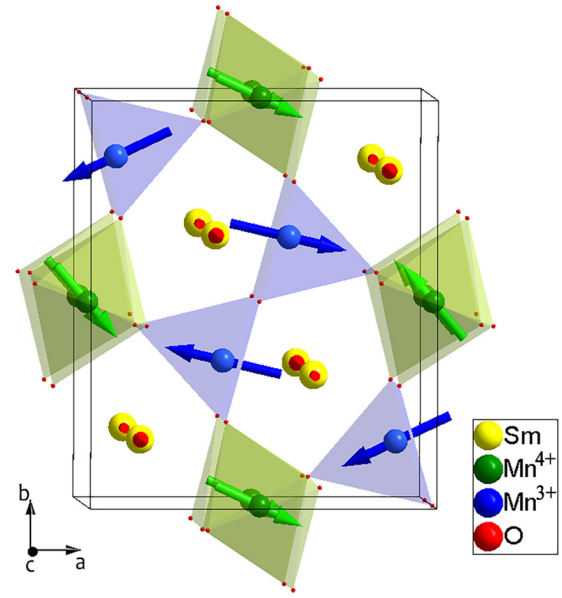

FIG. 10. Magnetic structure of $SmMn_2O_5$ at 32 K and 10.3 GPa. The moments of Sm^{3+} are along the c axis. The amplitude of the moments of Sm^{3+} are multiplied by a factor of 2 for the sake of clarity.

C. $NdMn_2O_5$

At ambient pressure and below ~40 K, the main magnetic phase of $NdMn_2O_5$ is an ICM phase with propagation wave vector $\mathbf{q}_{ICM} = (\frac{1}{2}, 0, \frac{2}{5} - \delta)$. At low temperature, below ~5 K, a weak additional CM phase coexists with the main ICM phase [18]. Under a weak pressure of about ~1.2 GPa, at low temperature the phase diagram is unchanged. However, above ~5, we observe the appearance of the same PCM phase [$\mathbf{q}_{PCM} = (\frac{1}{2}, 0, \frac{1}{2})$] as observed in the other members of the RMn_2O_5 family. It coexists with the ICM phase below 2.8 GPa. Finally, the ICM phase totally disappears above 2.8 GPa. With further increasing the pressure, at low temper-

TABLE II. Refinement results for the PCM structure of $SmMn_2O_5$ at 32 K and 10.3 GPa in $P-1$ space group with $\chi^2 = 52.9$, $R_p = 47.6\%$, $R_{wp} = 25.6\%$, $R_{exp} = 3.5\%$, $R_{bragg} = 2.5\%$, and $R_{mag} = 34.1\%$. ϕ and θ refer to the polar angle and the azimuthal angle, respectively.

Atom	x	y	z	$M(\mu_B)$	ϕ (°)	θ (°)
Sm^{3+}	0.1419	0.1709	0	0.7(6)	–	0
	0.3580	0.6709	0	0.7(6)	–	0
	0.6419	0.3290	0	0.7(6)	–	0
	0.8580	0.8290	0	0.7(6)	–	0
Mn^{3+}	0.4045	0.3488	0.5	2.5(5)	−193.9(0)	90
	0.5954	0.6511	0.5	2.5(5)	−13.9(1)	90
	0.0954	0.8488	0.5	2.5(5)	−158.7(7)	90
	0.9045	0.1511	0.5	2.5(5)	−158.7(7)	90
Mn^{4+}	0	0.5	0.2490	2.0(0)	−45.6(9)	90
	0	0.5	0.7509	2.0(0)	−45.6(8)	90
	0	0.5	0.2490	2.0(0)	−21.0(6)	90
	0	0.5	0.7509	2.0(0)	−21.0(7)	90

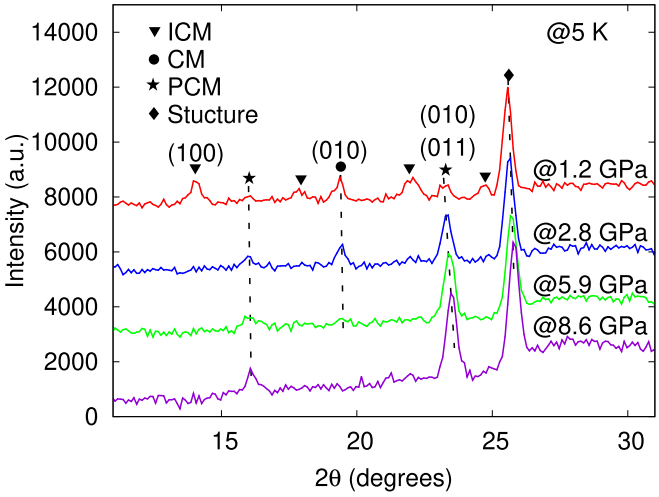

FIG. 11. $NdMn_2O_5$. Pressure evolution of the main reflections of the ICM (100), CM (010), and PCM [(010) and (011)] at the lowest temperature, 5 K.

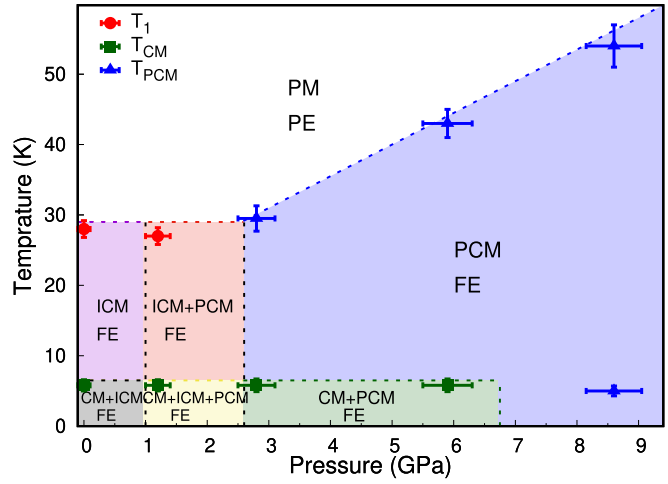

FIG. 13. Pressure–temperature (*P–T*) phase diagram of $NdMn_2O_5$ deduced from our neutron-diffraction experiments.

ature (∼5 K) the PCM phase becomes more intense at the expense of the CM phase. At 8.6 GPa, the CM phase has totally disappeared and the PCM phase is the unique magnetic phase. The pressure evolution of the diffractograms at the lowest temperature, ∼5 K, is illustrated in Fig. 11. At 5 K, the coexistence between the ICM, CM, and PCM phases has been studied as for $SmMn_2O_5$. The balance between the ICM, CM, and PCM phases calculated from the integrated intensity of the main magnetic reflection of each phase is shown in Fig. 12 as a function of the pressure. The $(P-T)$ phase diagram is summarized in Fig. 13.

The magnetic structure has been refined in the PCM phase at the lowest temperature (5 K) and the highest pressure (8.6 GPa). As for $GdMn_2O_5$, we choose the *planar* model to refine the PCM phase because the magnetic easy plane is expected to remain in the (*a, b*) plane under pressure. We mainly refined the direction of the moments starting from their orientation in the CM phase at ambient pressure. The intensity of the magnetic reflections being very strong, the accuracy of our fit of the data is quite high. The best fit is shown in Fig. 14. The corresponding magnetic structure of the PCM phase is given in Fig. 15. The refined parameters of $NdMn_2O_5$ at 5 K and 8.6 GPa are listed in Table III. The orientation of the Mn spins are roughly along *a* whereas the ordered moments of the Nd^{3+} moments are very small and along the *b* axis. This seems to indicate that the magnetic easy axis of the Nd^{3+} moments is along *b*. This is consistent with the magnetization measurements performed on single crystal for $NdMn_2O_5$ [18], showing a slight decrease of the magnetization along *b* below ∼5 K, which is the critical temperature attributed to the Nd^{3+} spins ordering.

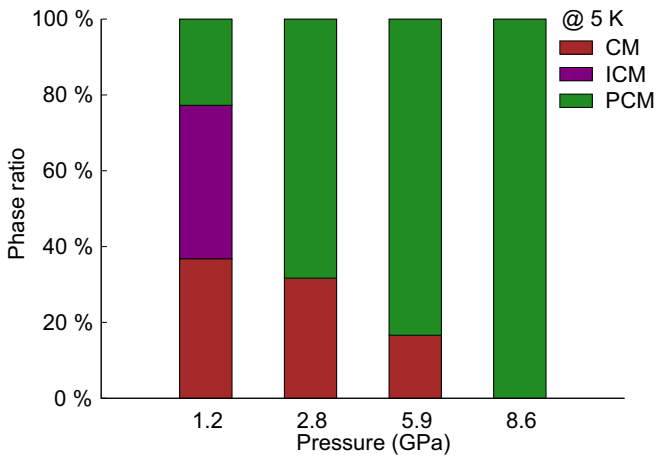

FIG. 12. $NdMn_2O_5$. Pressure evolution of phase ratio of the ICM, CM, and PCM phases at 5K.

IV. DISCUSSION

For all the compounds studied in this paper, the phase diagrams Figs. 4, 8, and 13 have evidenced a new PCM

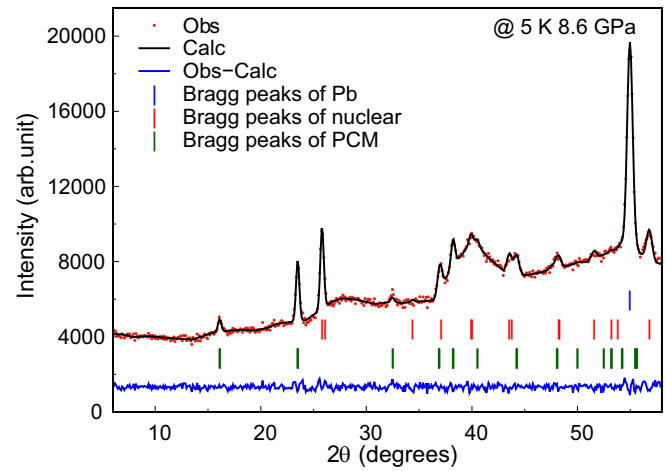

FIG. 14. Diffractogram of $NdMn_2O_5$ at the lowest temperature, 5 K, and highest pressure, 8.6 GPa, where the PCM phase is present alone. The reflection of the Pb is used to calculate the exact pressure inside the gasket.

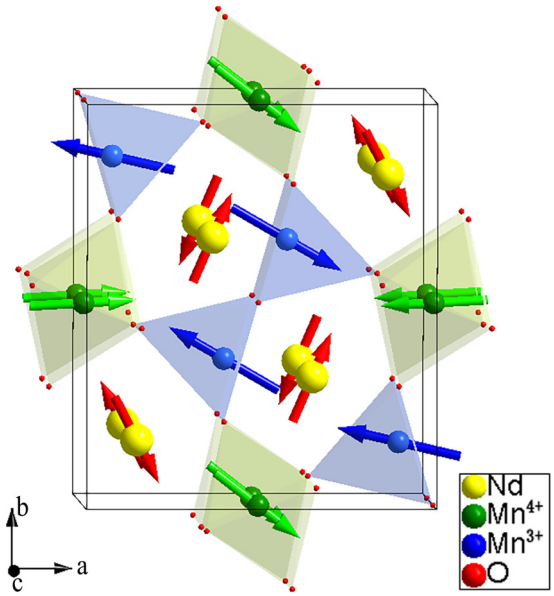

FIG. 15. Magnetic structure of $NdMn_2O_5$ at 5 K and 8.6 GPa. The amplitude of the moments of Nd^{3+} are multiplied by a factor of 2 for the sake of clarity.

phase. This PCM phase generally grows under pressure at the expense of the ICM phase observed at HT. At HT and high pressure, the PCM phase totally replaces the ICM phase. On the other hand, at low temperature, the PCM phase competes with the CM phase under pressure. They coexist in a large part of the (P–T) phase diagram due to the high stability of the CM(p) phase, which is ascribed to the additional magnetic ordering of the R^{3+}. As a consequence, for $GdMn_2O_5$ and $SmMn_2O_5$ with a dominant CM phase at ambient pressure, the PCM phase is stabilized only at high pressure (4–5 GPa) and HT. As for $NdMn_2O_5$, stabilizing mainly an ICM phase at ambient pressure, the PCM phase appears already at very low pressure and exists alone in the entire temperature range above 6 GPa.

TABLE III. Refinement results for the PCM structure of $NdMn_2O_5$ at 5 K, 8.6 GPa in $P1$ space group with $\chi^2 = 87.7$, $R_p = 32.9\%$, $R_{wp} = 14.5\%$, $R_{\text{exp}} = 1.55\%$, $R_{\text{bragg}} = 0.9\%$ and $R_{\text{mag}} = 8.1\%$. ϕ and θ refer to the polar angle and the azimuthal angle, respectively.

Atom	x	y	z	$M(\mu_B)$	ϕ (°)	θ (°)
Nd^{3+}	0.1428	0.1721	0	0.9(9)	118.2(1)	90
	0.3571	0.6722	0	0.9(9)	242.2(1)	90
	0.6428	0.3278	0	0.9(9)	242.2(1)	90
	0.8571	0.8278	0	0.9(9)	118.2(1)	90
Mn^{3+}	0.4098	0.3528	0.5	2.6(7)	−210.1(1)	90
	0.5901	0.6471	0.5	2.6(7)	−30.1(1)	90
	0.0901	0.8528	0.5	2.6(7)	−191.8(4)	90
	0.9098	0.1471	0.5	2.6(7)	−191.8(4)	90
Mn^{4+}	0	0.5	0.2567	2.2(6)	0.6(7)	90
	0	0.5	0.7433	2.2(6)	0.6(7)	90
	0	0.5	0.2567	2.2(6)	−33.6(9)	90
	0	0.5	0.7433	2.2(6)	−33.6(9)	90

TABLE IV. Moments of R^{3+} at the highest pressure, ∼8 ± 2 GPa, at different temperatures.

R	Moment (μ_B)
Pr [25]	0 (@ 6 K)
Dy [26]	0.4 (@ 18 K)
Tb [26]	1.0 (@ 20 K)
Gd	0.2 (@ 32 K)
Sm	0.5 (@ 32 K)
Nd	0.9 (@ 5 K)

For all the compounds studied here, the new PCM phase is associated with the same propagation wave vector $\mathbf{q}_{\text{PCM}} = (\frac{1}{2}, 0, \frac{1}{2})$, similar to the one previously evidenced in YMn_2O_5 [23], $PrMn_2O_5$ [25], $TbMn_2O_5$, and $DyMn_2O_5$ [26] under pressure. It is important to mention that the propagation wave vector of the PCM phase ($\mathbf{q}_{\text{PCM}}$) is universal for the various compounds of the series despite their different magnetic propagation wave vectors at ambient pressure. Another universal character of the PCM phases is the small value of the ordered R^{3+} moments. Table IV summarizes the values of the R^{3+} moments for the various PCM phases. Interestingly, a small ordered moment of the rare earth leads to a J_6 term in the Hamiltonian.

A mechanism for the stabilization of the PCM phase has been proposed in Ref. [26] for $TbMn_2O_5$ and $DyMn_2O_5$. It is based on the analysis that the unique difference between the propagation wave vectors of the various magnetic phases in these compounds is related to the c component, namely k_z. Focusing on this direction and using a toy model, we represent the magnetic structure as chains of R^{3+}, Mn^{3+}, and Mn^{4+} spins running along the c direction and coupled by various exchange interactions as shown in Fig. 16. Within this model, one can calculate the magnetic energy in the different competing magnetic phases. The calculation shows for all the compounds studied here that the PCM phase with $k_z = 1/2$ is stabilized by a strong J_1 exchange interaction and that the CM phase with $k_z = 0$ is stabilized by a strong J_6 interaction.

At ambient pressure, the J_6 term seems to be strong enough to overcome the J_1 term, either because of a strong J_6 coupling itself or because of a large moment amplitude for the rare earth (as in the Gd case). This is only effective at low temperature at which the moment on the R^{3+} can order. As a consequence, an effective ferromagnetic order between Mn^{4+} along c sets in, which results in the stabilization of the CM phase. Under pressure, the shortening of the atomic distances leads to the increase of both J_1 and J_6. However, it is obvious regarding the (P–T) phase diagram that, under pressure, J_1 increases more than J_6, relatively. This stabilizes the PCM under pressure at least at HT. In turn, the presence of the PCM phase with generally small R^{3+} moments results in the reduction of the J_6 term and thus in turn further stabilizes the PCM phase. This general scenario is in perfect agreement with all the results obtained in $GdMn_2O_5$, $SmMn_2O_5$, and $NdMn_2O_5$. In the particular case of $NdMn_2O_5$, it is interesting to notice that due to the small Nd^{3+} moments and a weak J_6 term, no CM phase really develops even at ambient pressure. Under pressure, the PCM phase dominates in the entire phase diagram.

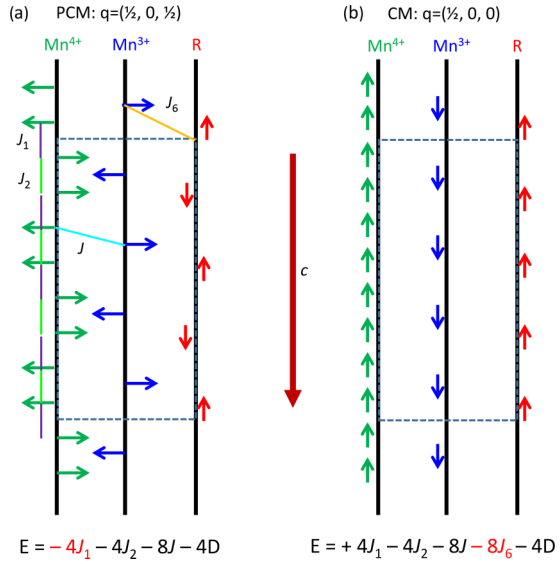

FIG. 16. Schematic magnetic structure of $R\mathrm{Mn_2O_5}$ (in the particular case of $R = Sm$) with 1D chains. To simplify the model, J_4 and J_5 are replaced by an effective $\mathrm{Mn^{4+} - Mn^{3+}}$ interaction, J. The magnetic energy for the different magnetic orders k_z is calculated for (a) $k_z = \frac{1}{2}$ (for the PCM phase) and (b) $k_z = 0$ (for the CM phase). In the expressions of the energy, D corresponds to the anisotropy term due to the Ising-like anisotropy of the R ions.

This interpretation for the stabilization of the PCM phase stands for compounds with magnetic R^{3+} ions because they have a finite J_6 coupling. For systems with nonmagnetic rare earth such as $\mathrm{BiMn_2O_5}$ or $\mathrm{YMn_2O_5}$, the strong J_1 interaction by itself can also explain the stabilization of the PCM phase under high pressure. Indeed, this thus implies that the order between two successive $\mathrm{Mn^{4+}}$ through J_1 is AFM while the order between $\mathrm{Mn^{4+}}$ through J_2 is always ferromagnetic because J_2 is frustrated by the strong $\mathrm{Mn^{3+} - Mn^{4+}}$ exchange interactions (J_3 and J_4) [33]. However, our simple mechanism considering only J_1 and J_6 is not enough to understand the ambient and low-pressure phase diagram of $\mathrm{YMn_2O_5}$ [24,34]. The introduction of a J_{12} next-nearest-neighbor exchange interaction between $\mathrm{Mn^{4+}}$ seems to be necessary to explain the k_z component [35,36].

It is interesting to look further on the multiferroic properties of the $R\mathrm{Mn_2O_5}$ under pressure. Previous polarization measurements have evidenced the enhancement of the electric polarization under pressure in Refs. [37,38]. Furthermore a connection between the enhancement of the electric polarization and the appearance of the PCM phase has been established in Ref. [23]. However, the polarization has been measured at small pressure at which the PCM phase usually coexists with other magnetic phase(s). It would thus be of great interest to investigate the ferroelectric character of the PCM phase alone by measuring the polarization at high pressure. According to the magnetic structures we proposed for the PCM phase with a quasicollinear spin arrangement, and following the exchange-striction mechanism, the PCM phase is expected to be of high polarization. In the particular case of $\mathrm{NdMn_2O_5}$ with a minute polarization at ambient pressure, we expect a colossal enhancement of the polarization under pressure.

V. CONCLUSION

In conclusion, we showed that external pressure is a powerful tool to modify the magnetic properties in the $R\mathrm{Mn_2O_5}$ multiferroic family in a universal manner. The pressure-induced commensurate phase seems to be in connection with an enhancement of its ferroelectric properties. Despite a complex magnetic phase diagram and numerous exchange terms, the mechanism which accounts for the modifications of the magnetic order can be understood, considering a simple competition between two particular exchange terms. This result may open the possibility to predict the effect of pressure on the multiferroic properties of this complex family of materials by estimation of two exchange interactions.

ACKNOWLEDGMENTS

This work was supported by the Chinese Scholarship Council project. The work of M. Greenblatt at Rutgers was supported by NSF-DMR Grant No. 1507252.

[1] H. Schmid, Ferroelectrics **162**, 317 (1994).
[2] M. Fiebig, J. Phys. D: Appl. Phys. **38**, R123 (2005).
[3] S. W. Cheong and M. Mostovoy, Nat. Mater. **6**, 13 (2007).
[4] V. Balédent, S. Chattopadhyay, P. Fertey, M. B. Lepetit, M. Greenblatt, B. Wanklyn, F. O. Saouma, J. I. Jang, and P. Foury-Leylekian, Phys. Rev. Lett. **114**, 117601 (2015).
[5] S. Chattopadhyay, S. Petit, E. Ressouche, S. Raymond, V. Balédent, G. Yahia, W. Peng, J. Robert, M.-B. Lepetit, M. Greenblatt, and P. Foury-Leylekian, Sci. Rep. **7**, 14506 (2017).
[6] N. Hur, S. Park, P. A. Sharma, J. S. Ahn, S. Guha, and S.-W. Cheong, Nature **429**, 392 (2004).
[7] G. Yahia, F. Damay, S. Chattopadhyay, V. Balédent, W. Peng, E. Elkaim, M. Whitaker, M. Greenblatt, M.-B. Lepetit, and P. Foury-Leylekian, Phys. Rev. B **95**, 184112 (2017).
[8] V. Polyakov, V. Plakhty, M. Bonnet, P. Burlet, L.-P. Regnault, S. Gavrilov, I. Zobkalo, and O. Smirnov, Phys. B: Condens. Matter **297**, 208 (2001).
[9] G. Yahia, F. Damay, S. Chattopadhyay, V. Balédent, W. Peng, S. W. Kim, M. Greenblatt, M.-B. Lepetit, and P. Foury-Leylekian, Phys. Rev. B **97**, 085128 (2018).
[10] L. C. Chapon, G. R. Blake, M. J. Gutmann, S. Park, N. Hur, P. G. Radaelli, and S.-W. Cheong, Phys. Rev. Lett. **93**, 177402 (2004).
[11] G. R. Blake, L. C. Chapon, P. G. Radaelli, S. Park, N. Hur, S.-W. Cheong, and J. Rodríguez-Carvajal, Phys. Rev. B **71**, 214402 (2005).
[12] P. P. Gardner, C. Wilkinson, J. B. Forsyth, and B. M. Wanklyn, J. Phys. C: Solid State Phys. **21**, 5653 (1988).
[13] M. Uga, N. Iwata, and K. Kohn, Ferroelectrics **219**, 55 (1998).
[14] Y. Koyata, H. Nakamura, N. Iwata, A. Inomata, and K. Kohn, J. Phys. Soc. Jpn. **65**, 1383 (1996).
[15] I. Kagomiya and K. Kohn, Ferroelectrics **219**, 169 (1998).

[16] A. Muñoz, J. A. Alonso, M. T. Casais, M. J. Martínez-Lope, J. L. Martínez, and M. T. Fernández-Díaz, Eur. J. Inorg. Chem. **2005**, 685 (2005).

[17] C. Doubrovsky, G. André, A. Gukasov, P. Auban-Senzier, C. R. Pasquier, E. Elkaim, M. Li, M. Greenblatt, F. Damay, and P. Foury-Leylekian, Phys. Rev. B **86**, 174417 (2012).

[18] S. Chattopadhyay, V. Balédent, F. Damay, A. Gukasov, E. Moshopoulou, P. Auban-Senzier, C. Pasquier, G. André, F. Porcher, E. Elkaim, C. Doubrovsky, M. Greenblatt, and P. Foury-Leylekian, Phys. Rev. B **93**, 104406 (2016).

[19] N. Lee, C. Vecchini, Y. J. Choi, L. C. Chapon, A. Bombardi, P. G. Radaelli, and S.-W. Cheong, Phys. Rev. Lett. **110**, 137203 (2013).

[20] T. Fujita and K. Kohn, Ferroelectrics **219**, 155 (1998).

[21] N. Hur, S. Park, P. A. Sharma, S. Guha, and S.-W. Cheong, Phys. Rev. Lett. **93**, 107207 (2004).

[22] J. W. Kim, S. Y. Haam, Y. S. Oh, S. Park, S.-W. Cheong, P. A. Sharma, M. Jaime, N. Harrison, J. H. Han, G.-S. Jeon, P. Coleman, and K. H. Kim, Proc. Natl. Acad. Sci. USA **106**, 15573 (2009).

[23] M. Deutsch, T. C. Hansen, M. T. Fernandez-Diaz, A. Forget, D. Colson, F. Porcher, and I. Mirebeau, Phys. Rev. B **92**, 060410(R) (2015).

[24] D. P. Kozlenko, N. T. Dang, S. E. Kichanov, E. V. Lukin, A. M. Pashayev, A. I. Mammadov, S. H. Jabarov, L. S. Dubrovinsky, H.-P. Liermann, W. Morgenroth, R. Z. Mehdiyeva, V. G. Smotrakov, and B. N. Savenko, Phys. Rev. B **92**, 134409 (2015).

[25] W. Peng, V. Balédent, S. Chattopadhyay, M.-B. Lepetit, G. Yahia, C. V. Colin, M. J. Gooch, C. R. Pasquier, P. Auban-Senzier, M. Greenblatt, and P. Foury-Leylekian, Phys. Rev. B **96**, 054418 (2017).

[26] M. Deutsch, W. Peng, P. Foury-Leylekian, V. Balédent, S. Chattopadhyay, M. T. Fernandez-Diaz, T. C. Hansen, A. Forget, D. Colson, M. Greenblatt, M.-B. Lepetit, S. Petit, and I. Mirebeau, Phys. Rev. B **98**, 024408 (2018).

[27] N. T. Dang, D. P. Kozlenko, S. E. Kichanov, S. G. Jabarov, A. I. Mammadov, R. Z. Mekhtieva, T. L. Phan, V. G. Smotrakov, V. V. Eremkin, and B. N. Savenko, J. Electron. Mater. **46**, 3373 (2017).

[28] H. Kimura, K. Nishihata, Y. Noda, N. Aso, K. Matsubayashi, Y. Uwatoko, and T. Fujiwara, J. Phys. Soc. Jpn. **77**, 063704 (2008).

[29] W. Peng, V. Balédent, S. Chattopadhyay, P. Foury Leylekian, T. Hansen, and G. Yahia, $^{160}GdMn_2O_5$ under pressure, a good candidate for multiferroics, Institut Laue-Langevin (ILL), Cycles: 20181, https://doi.org/10.5291/ILL-DATA.5-31-2558 (2018).

[30] W. Peng, V. Balédent, C. Colin, and P. Foury Leylekian, $^{154}SmMn_2O_5$ under pressure, a good candidate for multiferroics, Institut Laue-Langevin (ILL), Cycles: 20181, https://doi.org/10.5291/ILL-DATA.CRG-2501 (2018).

[31] W. Peng, C. Colin, P. Foury Leylekian, and A. Vaunat, $NdMn_2O_5$ under pressure, a good canditdate for multiferroics, Institut Laue-Langevin (ILL), Cycles: 20181, https://doi.org/10.5291/ILL-DATA.CRG-2451 (2018).

[32] J. Rodríguez-Carvajal, Phys. B: Condens. Matter **192**, 55 (1993).

[33] W. Peng, V. Balédent, M.-B. Lepetit, A. Vaunat, E. Rebolini, M. Greenblatt, and P. Foury-Leylekian, Acta Crystallogr. Sect. B (to be published).

[34] L. C. Chapon, P. G. Radaelli, G. R. Blake, S. Park, and S.-W. Cheong, Phys. Rev. Lett. **96**, 097601 (2006).

[35] P. G. Radaelli and L. C. Chapon, J. Phys.: Condens. Matter **20**, 434213 (2008).

[36] J.-H. Kim, M. A. van der Vegte, A. Scaramucci, S. Artyukhin, J. H. Chung, S. Park, S.-W. Cheong, M. Mostovoy, and S. H. Lee, Phys. Rev. Lett. **107**, 097401 (2011).

[37] C. R. dela Cruz, B. Lorenz, Y. Y. Sun, Y. Wang, S. Park, S. W. Cheong, M. M. Gospodinov, and C. W. Chu, Phys. Rev. B **76**, 174106 (2007).

[38] R. P. Chaudhury, C. R. dela Cruz, B. Lorenz, Y. Sun, C.-W. Chu, S. Park, and S.-W. Cheong, Phys. Rev. B **77**, 220104(R) (2008).